Inorg. Chem. **2007**, *46*, 8410–8417

Inorganic Chemistry

Article

X-ray Absorption Spectroscopic Studies of High-Spin Nonheme (Alkylperoxo)iron(III) Intermediates

Xiaopeng Shan,[†] Jan-Uwe Rohde,[†,‡] Kevin D. Koehntop,[†,‡] Yuming Zhou,[†] Michael R. Bukowski,[†,‡] Miquel Costas,[†,‡] Kiyoshi Fujisawa,[‡] and Lawrence Que Jr.*,[†]

Department of Chemistry and Center for Metals in Biocatalysis, University of Minnesota, Minneapolis, Minnesota 55455, and Department of Chemistry, University of Tsukuba, Tsukuba 305-8571, Japan

Received April 5, 2007

The reactions of iron(II) complexes [Fe(Tp$^{t-\mathrm{Bu},i-\mathrm{Pr}}$)(OH)] (**1a**, Tp$^{t-\mathrm{Bu},i-\mathrm{Pr}}$ = hydrotris(3-*tert*-butyl-5-isopropyl-1-pyrazolyl)-borate), [Fe(6-Me_2BPMCN)$(OTf)_2$] (**1b**, 6-Me_2BPMCN = *N*,*N*′-bis((2-methylpyridin-6-yl)methyl)-*N*,*N*′-dimethyl-*trans*-1,2-diaminocyclohexane), and [Fe(L^8Py_2)(OTf)](OTf) (**1c**, L^8Py_2 = 1,5-bis(pyridin-2-ylmethyl)-1,5-diazacyclooctane) with *tert*-BuOOH give rise to high-spin Fe^{III}–OOR complexes. X-ray absorption spectra (XAS) of these high-spin species show characteristic features, distinct from those of low-spin Fe–OOR complexes (Rohde, J.-U.; et al. *J. Am. Chem. Soc.* **2004**, *126*, 16750–16761). These include (1) an intense 1s → 3d preedge feature, with an area around 20 units, (2) an edge energy, ranging from 7122 to 7126 eV, that is affected by the coordination environment, and (3) a 1.86–1.96 Å Fe–OOR bond, compared to the 1.78 Å Fe–OOR bond in low-spin complexes. These unique features likely arise from a flexible first coordination sphere in those complexes. The difference in Fe–OOR bond length may rationalize differences in reactivity between low-spin and high-spin Fe^{III}–OOR species.

Introduction

Many nonheme iron enzymes carry out metabolically important oxidative transformations by activating dioxygen.[1−4] Proposed mechanisms of several mononuclear and dinuclear nonheme iron enzymes involve high-spin iron(III)−peroxo species, namely Fe^{III}−OOR(H) or Fe^{III}−OO−Fe^{III}, as intermediates that undergo O−O bond cleavage to become high-valent species,[2,3] e.g. Fe^{IV}=O for 1-aminocyclopropane-1-carboxylate oxidase,[5] Fe^{V}(O)(OH) for Rieske dioxygenases,[2] $Fe^{IV}_2(\mu\text{-O})_2$ for methane monooxygenase,[6] and Fe^{III}−O−Fe^{IV} for ribonucleotide reductase.[7] On the other hand, the catalytic cycles of lipoxygenase and superoxide reductase[8,9] involve formation of high-spin Fe^{III}−OOR(H) species and then release of ROOH or H_2O_2 through Fe−O bond cleavage. To understand the factors that control this two-sided reactivity, structural information of these Fe^{III}−peroxo intermediates is essential.

So far, several high-spin Fe^{III}−OOR(H) intermediates have been crystallographically characterized for nonheme enzymes, the purple end-on bound alkylperoxo intermediate of soybean lipoxygenase-3[9] and the side-on bound O_2 adducts of naphthalene dioxygenase in the presence and in the absence of substrate.[10] The limited structural information available from nonheme iron enzymes makes studies of Fe−OOR(H) model complexes quite important. A number of such synthetic complexes have been obtained with a variety

---

* To whom correspondence should be addressed. E-mail: que@chem.umn.edu.

[†] University of Minnesota.

[‡] Current addresses: Department of Chemistry, The University of Iowa, Iowa City, IA 52242 (J.-U.R.); The Scripps Research Institute, La Jolla, CA 92037 (K.K.); Penn State Altoona, Altoona, PA 16601 (M.R.B.); University of Tsukuba. Departament de Química and Institut de Química Computacional, Universitat de Girona, Campus de Montilivi E-17071, Girona, Spain (M.C.).

(1) Abu-Omar, M. M.; Loaiza, A.; Hontzeas, N. *Chem. Rev.* **2005**, *105*, 2227−2252.
(2) Costas, M.; Mehn, M. P.; Jensen, M. P.; Que, L., Jr. *Chem. Rev.* **2004**, *104*, 939−986.
(3) Merkx, M.; Kopp, D. A.; Sazinsky, M. H.; Blazyk, J. L.; Muller, J.; Lippard, S. J. *Angew. Chem., Int. Ed.* **2001**, *40*, 2782−2807.
(4) Solomon, E. I.; Brunold, T. C.; Davis, M. I.; Kemsley, J. N.; Lee, S.-K.; Lehnert, N.; Neese, F.; Skulan, A. J.; Yang, Y.-S.; Zhou, J. *Chem. Rev.* **2000**, *100*, 235−349.
(5) Rocklin, A. M.; Kato, K.; Liu, H.-w.; Que, L.; Lipscomb, J. D. *J. Biol. Inorg. Chem.* **2004**, *9*, 171−182.
(6) Shu, L.; Nesheim, J. C.; Kauffmann, K.; Munck, E.; Lipscomb, J. D.; Que, L., Jr. *Science* **1997**, *275*, 515−518.
(7) Sturgeon, B. E.; Burdi, D.; Chen, S.; Huynh, B.-H.; Edmondson, D. E.; Stubbe, J.; Hoffman, B. M. *J. Am. Chem. Soc.* **1996**, *118*, 7551−7557.
(8) (a) Kurtz, D. M. *J. Inorg. Biochem.* **2006**, *100*, 679−693. (b) Katona, G.; Carpentier, P.; Niviere, V.; Amara, P.; Adam, V.; Ohana, J.; Tsanov, N.; Bourgeois, D. *Science* **2007**, *316*, 449−453.
(9) Skrzypczak-Jankun, E.; Bross, R. A.; Carroll, R. T.; Dunham, W. R.; Funk, M. O., Jr. *J. Am. Chem. Soc.* **2001**, *123*, 10814−10820.
(10) Karlsson, A.; Parales, J. V.; Parales, R. E.; Gibson, D. T.; Eklund, H.; Ramaswamy, S. *Science* **2003**, *299*, 1039−1042.

10.1021/ic700649w CCC: $37.00

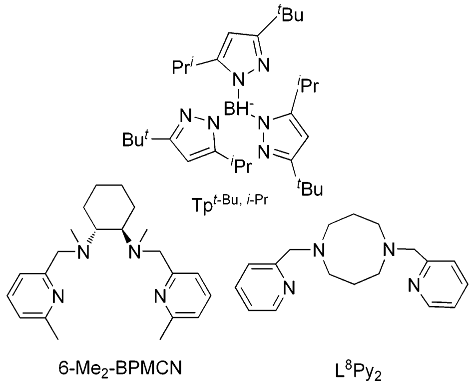

Figure 1. Ligands utilized in XAS studies of high-spin (alkylperoxo)-iron(III) complexes.

of polydentate ligands.[2] Several low-spin Fe−OOR(H) complexes decompose to form high-valent oxoiron(IV) species,[11−13] and structural insight into these complexes has been obtained by X-ray absorption spectroscopy (XAS).[14] So far, the transformation of high-spin Fe^{III}−OOR(H) species into high-valent iron species has not been reported. DFT calculations strongly suggested that high-spin Fe^{III}−OOR-(H) species prefer the pathway of Fe−O bond cleavage instead of O−O bond lysis that does occur in catalytic cycles of nonheme iron enzymes.[15] To further rationalize this discrepancy and understand the effect of the structure on the reactivity of high-spin Fe^{III}−OOR species, we successfully generated four high-spin Fe^{III}−OOR species supported by ligands depicted in Figure 1 and carried out X-ray absorption spectroscopic (XAS) studies. Comparison of our current results with previously published low-spin ones provides essential structural information on these Fe^{III}−OOR species and may reveal how the structure and spin state affect the reactivity of these Fe^{III}−OOR(H) species.

Experimental Section

Materials and General Procedures. All reagents and solvents were purchased from commercial sources and used as received, unless noted otherwise. Solvents were dried according to published procedures and distilled under Ar prior to use.[16] Preparation and handling of air-sensitive materials were carried out under an inert atmosphere by using either standard Schlenk and vacuum line techniques or a glovebox.

Preparation of Iron(II) Precursors. $[Fe(Tp^{t-Bu,i-Pr})(OH)]$,[17] **1a**, $[Fe(6\text{-}Me_2BPMCN)(OTf)_2]$,[18] **1b**, and $[Fe(L^8Py_2)(OTf)](OTf)$,[19] **1c**, were synthesized according to published procedures.

XAS Sample Preparation. Samples of (alkylperoxo)iron(III) intermediates **2a**−**c** and **2c′** were generated by adding *tert*-BuOOH to precooled solutions of the respective iron(II) precursors. After a suitable period of reaction time during which the chromophore was observed to maximize by UV−visible spectroscopy, ca. 0.5 mL of the solution was transferred into a precooled sample holder, covered with Mylar tape, and submerged in liquid nitrogen.

$[Fe^{III}(Tp^{t-Bu,\ i-Pr})(OO^tBu)]^+$, 2a. A 10 equiv amount of *tert*-BuOOH (5.0−6.0 M in decane) was added into a solution of 10 mM **1a** in diethyl ether, precooled to −80 °C. After 1 h, maximum absorption of the chromophore at 510 nm ($\epsilon = 700\ M^{-1}\ cm^{-1}$) was reached, corresponding to a yield of **2a** of above 95%.

$[Fe^{III}(6\text{-}Me_2BPMCN)(solv)(OO^tBu)]^{2+}$, 2b. A 25 equiv amount of *tert*-BuOOH (5.0−6.0 M in decane) was added into a solution of 10 mM **1b** in butyronitrile, precooled to −60 °C. After 0.5 h, maximum absorption of the chromophore at 587 nm ($\epsilon = 2600\ M^{-1}\ cm^{-1}$) was reached, corresponding to a yield of **2b** of around 90%.

$[Fe^{III}(L^8Py_2)(solv)(OO^tBu)]^{2+}$, 2c. A 10 equiv amount of *tert*-BuOOH (5.0−6.0 M in decane) was added into a solution of 10 mM **1c** in butyronitrile, precooled to −80 °C. After 0.5 h, maximum absorption of the chromophore at 580 nm ($\epsilon = 2500\ M^{-1}\ cm^{-1}$) was reached, corresponding to a yield of **2c** of ca. 80%.

$[Fe^{III}(L^8Py_2)(OPy)(OO^tBu)]^{2+}$, 2c′. A 10 equiv amount of *tert*-BuOOH (5.0−6.0 M in decane) was added into a solution of 5 mM **1c** in butyronitrile, precooled to −80 °C. With the addition of 5 equiv of PyO, **2c′** was generated in 90% yield based upon the absorption of the chromophore at 550 nm ($\epsilon = 2100\ M^{-1}\ cm^{-1}$).

Physical Methods. UV−visible spectra were recorded on an HP 8453A diode array spectrometer with samples maintained at low temperature using a cryostat from Unisoku Scientific Instruments, Osaka, Japan.

X-ray Absorption Spectroscopy. Data Collection. XAS data were collected on beamline 9-3 at the Stanford Synchrotron Radiation Laboratory (SSRL) of the Stanford Linear Accelerator Center and on beamline X9B at the National Synchrotron Light Source (NSLS) of the Brookhaven National Laboratory. Fe K-edge X-ray absorption spectra were recorded on frozen solutions at 5−15 K over the energy range 6.9−8.0 keV as described previously.[20,21] Storage ring conditions: 3 GeV, 50−100 mA (SSRL); 2.8 GeV, 100−300 mA (NSLS). Contamination of higher harmonics radiation was minimized by detuning the Si(220) double-crystal monochromator by 50% at ca. 8 keV (beamline 9-3 at SSRL) and by a harmonic rejection mirror (beamline X9B at NSLS), respectively. The horizontal spot size on the sample was 4−5 mm in most cases. Spectra were measured with 10 eV steps below the edge, 0.3 eV steps in the edge region, and steps equivalent to 0.05 $Å^{-1}$ increments above the edge (region borders were 6880, 7090, and 7140 eV at beamline 9-3, SSRL, and 6932, 7102, and 7137 eV at beamline X9B, NSLS). An iron foil spectrum was concomitantly recorded for internal energy calibration, and the first inflection point of the K-edge was assigned to 7112.0 eV. The data were obtained as fluorescence excitation spectra ($A_{exp} = C_f/C_0$) using a solid-state germanium detector (Canberra). The number of scans collected for

---

(11) Jensen, M. P.; Costas, M.; Ho, R. Y. N.; Kaizer, J.; Payeras, A. M.; Münck, E.; Que, L., Jr.; Rohde, J.-U.; Stubna, A. *J. Am. Chem. Soc.* **2005**, *127*, 10512−10525.

(12) Mairata i Payeras, A.; Ho, R. Y. N.; Fujita, M.; Que, L., Jr. *Chem. Eur. J.* **2004**, *10*, 4944−4953.

(13) Kaizer, J.; Costas, M.; Que, L., Jr. *Angew. Chem. Int. Ed.* **2003**, *42*, 3671−3673.

(14) Rohde, J.-U.; Torelli, S.; Shan, X.; Lim, M. H.; Klinker, E. J.; Kaizer, J.; Chen, K.; Nam, W.; Que, L., Jr. *J. Am. Chem. Soc.* **2004**, *126*, 16750−16761.

(15) Lehnert, N.; Ho, R. Y. N.; Que, L., Jr.; Solomon, E. I. *J. Am. Chem. Soc.* **2001**, *123*, 12802−12816.

(16) Armarego, W. L. F.; Perrin, D. D. *Purification of Laboratory Chemicals*; Butterworth-Heinemann: Oxford, U.K., 1997.

(17) Hikichi, S.; Ogihara, T.; Fujisawa, K.; Kitajima, N.; Akita, M.; Moro-oka, Y. *Inorg. Chem.* **1997**, *36*, 4539−4547.

(18) Costas, M.; Tipton, A. K.; Chen, K.; Jo, D.-H.; Que, L., Jr. *J. Am. Chem. Soc.* **2001**, *123*, 6722−6723.

(19) Halfen, J. A.; Moore, H. L.; Fox, D. C. *Inorg. Chem.* **2002**, *41*, 3935−3943.

(20) Scarrow, R. C.; Maroney, M. J.; Palmer, S. M.; Que, L., Jr.; Roe, A. L.; Salowe, S. P.; Stubbe, J. *J. Am. Chem. Soc.* **1987**, *109*, 7857−7864.

(21) Shu, L.; Chiou, Y.-M.; Orville, A. M.; Miller, M. A.; Lipscomb, J. D.; Que, L., Jr. *Biochemistry* **1995**, *34*, 6649−6659.

each sample were as follows: 12 scans for **2a** on beamline 9-3 at SSRL; 13 scans for **2b** on beamline X9B at NSLS; 10 scans for **2c** on beamline X9B; 18 scans for **2c′** on beamline 9-3.

Data Analysis. The treatment of raw EXAFS data to yield $\chi(k)$ is discussed in detail in review articles.[22,23] XAS data from beamline 9-3 at SSRL were calibrated and averaged with the program EXAFSPAK.[24] The resulting data were transferred to the program SSExafs and treated as XAS data from beamline X9B at NSLS.[20,25] Baseline subtraction and determination of the edge height were accomplished by fitting a cubic spline function (equally spaced throughout the EXAFS region) simultaneously with edge and EXAFS parameters (including first-shell parameters) and a correction of fluorescence data for thickness effects.

The edge was modeled as an integral of a 75% Gaussian and 25% Lorentzian peak. The heights, positions, and widths (at half-height) of preedge peaks were refined using a Gaussian function. Preedge peak areas are in % of Fe K-edge height × energy (eV) and were multiplied by 100.

The EXAFS refinements reported were on $k^3\chi(k)$ data, and the function minimized was $R = \{\Sigma k^6(\chi_c - \chi)^2/N\}^{1/2}$, where the sum is over N data points within the selected k space. Single-scattering EXAFS theory allows the total EXAFS spectrum to be described as the sum of shells of separately modeled atoms, e.g., $\chi_c = \Sigma nA[f(k)k^{-1}r^{-2}\exp(-2\sigma^2k^2)\sin(2kr + \alpha(k))]$, where n is the number of atoms in the shell, $k = [8\pi^2 m_e(E - E_0 + \Delta E)/h^2]^{1/2}$, and σ^2 is the Debye−Waller factor. The amplitude reduction factor (A) and the shell-specific edge shift (ΔE) are empirical parameters that partially compensate for imperfections in the theoretical amplitude and phase functions.[26] Phase and amplitude functions were theoretically calculated using a curved-wave formalism.[27] A variation of FABM (fine adjustment based on models) was used in the analysis procedure with theoretical phase and amplitude functions.[28] For each shell two parameters were refined (r and n or $\Delta\sigma^2$), while A (amplitude reduction factor) and ΔE (phase shift) values were determined using a series of crystallographically characterized model complexes. The fitting results indicate the average metal−ligand distances (r), the type and number of scatterers (n), and the Debye−Waller factors ($\Delta\sigma^2$, a difference between the σ^2 for the analyzed sample and the σ^2 for the model complexes), which can be used to evaluate the distribution of Fe−ligand bond lengths in each shell. The EXAFS goodness of fit criterion applied here is $\epsilon^2 = [(N_{idp}/\nu)\Sigma(\chi_c - \chi)^2/\sigma_{data}^2]/N$ as recommended by the International Committee on Standards and Criteria in EXAFS,[29,30] where ν is the number of degrees of freedom calculated as $\nu = N_{idp} - N_{var}$, N_{idp} is the number of independent data points, N_{var} is the number of variables that are refined, and σ_{data} is the estimated uncertainty of the data (usually set at 1). N_{idp} is calculated as $N_{idp} = 2\Delta k\Delta R/\pi + 2$.[31] The use of ϵ^2 as the criterion for the goodness of fit allows the comparison of fits using different numbers of variable parameters.

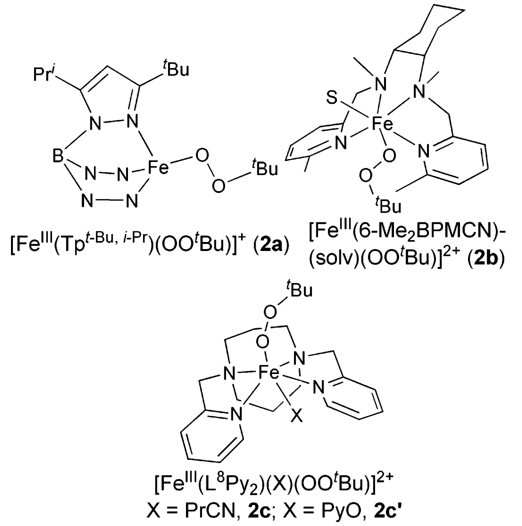

[Fe^{III}(Tp$^{t\text{-Bu},\,i\text{-Pr}}$)(OO^{t}Bu)]$^+$ (**2a**)

[Fe^{III}(6-Me$_2$BPMCN)-(solv)(OO^{t}Bu)]$^{2+}$ (**2b**)

[Fe^{III}(L^{8}Py$_2$)(X)(OO^{t}Bu)]$^{2+}$
X = PrCN, **2c**; X = PyO, **2c′**

Figure 2. Proposed structures of high-spin (alkylperoxo)iron(III) complexes.

Fitting Procedure. Fitting parameters A and ΔE for inner-sphere N/O and outer-sphere C scatterers had been extracted from Fe(acac)$_3$ (Fe−O, 1.986−2.004 Å; Fe···C, 2.935−2.971 Å).[20] Two of the parameters n, r, and $\Delta\sigma^2$ were allowed to float at the same time while the third parameter was fixed. The resolution was calculated from $\Delta r \cong \pi(2\Delta k)^{-1}$.[29] The typical error of analysis for interatomic distances (r) is approximately ±0.02 Å.[22,32]

Results and Discussion

In this study, we have obtained Fe K-edge X-ray absorption spectra of four high-spin (alkylperoxo)iron(III) complexes supported by tridentate or tetradentate ligands. XAS analysis affords essential structural information for these metastable complexes that is not currently available by X-ray crystallography. Comparison of these data with previously published results of corresponding low-spin complexes[14] allows the effect of iron spin state on the properties of the Fe^{III}−OOR unit to be determined.

Formation of High-Spin (Alkylperoxo)iron(III) Complexes. Iron(II) precursors **1a**−**c** react with *tert*-BuOOH at low temperature to form metastable high-spin (alkylperoxo)iron(III) complexes, [Fe^{III}(Tp$^{t\text{-Bu},i\text{-Pr}}$)(OO^{t}Bu)]$^+$, **2a**, [Fe^{III}(6-Me$_2$BPMCN)(solv)(OO^{t}Bu)]$^{2+}$, **2b**, and [Fe^{III}(L^{8}Py$_2$)(X)(OO^{t}Bu)]$^{2+}$, **2c**, in which X = solvent molecule (solv), as shown in Figure 2. Complex **2c′** for X = pyridine *N*-oxide (PyO) has been generated by introducing PyO into the solution of **2c**. Formation of the Fe^{III}−OOR moiety is indicated by the appearance of a prominent absorption band around 550 nm that can be attributed to the peroxo-to-iron LMCT transition.[33−38] All of these complexes show features indicative

---

(22) Scott, R. A. *Methods Enzymol.* **1985**, *117*, 414−459.
(23) Teo, B. K.; Joy, D. C. *EXAFS Spectroscopy: Techniques and Applications*; Plenum Press: New York, 1981.
(24) George, G. N.; Pickering, I. J. Stanford Synchrotron Radiantion Laboratory, Stanford Linear Accelerator Center, 2000.
(25) Scarrow, R. C.; Trimitsis, M. G.; Buck, C. P.; Grove, G. N.; Cowling, R. A.; Nelson, M. J. *Biochemistry* **1994**, *33*, 15023−15035.
(26) Teo, B.-K.; Lee, P. A. *J. Am. Chem. Soc.* **1979**, *101*, 2815−2832.
(27) McKale, A. G.; Veal, B. W.; Paulikas, A. P.; Chan, S. K.; Knapp, G. S. *J. Am. Chem. Soc.* **1988**, *110*, 3763−3768.
(28) Teo, B. K.; Antonio, M. R.; Averill, B. A. *J. Am. Chem. Soc.* **1983**, *105*, 3751−3762.
(29) Riggs-Gelasco, P. J.; Stemmler, T. L.; Penner-Hahn, J. E. *Coord. Chem. Rev.* **1995**, *144*, 245−286.
(30) Bunker, G. A.; Hasnain, S. S.; Sayers, D. E. *X-ray Absorption Fine Structure*; Ellis Horwood: New York, 1991.
(31) Stern, E. A. *Phys. Rev. B: Condens. Matter Mater. Phys.* **1993**, *48*, 9825−9827.
(32) Penner-Hahn, J. E. *Coord. Chem. Rev.* **1999**, *190−192*, 1101−1123.
(33) Nishida, Y.; Akamatsu, T. *Chem. Lett.* **1991**, 2013−2016.
(34) Zang, Y.; Kim, J.; Dong, Y.; Wilkinson, E. C.; Appelman, E. H.; Que, L., Jr. *J. Am. Chem. Soc.* **1997**, *119*, 4197−4205.
(35) Ogihara, T.; Hikichi, S.; Akita, M.; Uchida, T.; Kitagawa, T.; Moro-oka, Y. *Inorg. Chim. Acta* **2000**, *297*, 162−170.
(36) Kim, J.; Zang, Y.; Costas, M.; Harrison, R. G.; Wilkinson, E. C.; Que, L., Jr. *J. Biol. Inorg. Chem.* **2001**, *6*, 275−284.
(37) Lehnert, N.; Fujisawa, K.; Solomon, E. I. *Inorg. Chem.* **2003**, *42*, 469−481.

of $S = 5/2$ iron(III) centers in their EPR spectra. Raman vibrations associated with the $\mathrm{Fe^{III}{-}OOR(H)}$ moiety have been identified by ^{18}O-labeling studies, with the $\nu_{\mathrm{O-O}}$ near 900 cm^{-1} and the $\nu_{\mathrm{Fe-O}}$ near 600 cm^{-1}, as found for the previously characterized $[\mathrm{Fe^{III}(6\text{-}Me_3\text{-}TPA)(OO^{\mathit{t}}Bu)(solv)}]^{2+}$ intermediate.[15,34,39]

Coordination numbers of iron centers in these complexes range from 4 to 6, depending on the number of N donors on the polydentate ligand and the binding of the solvent molecule or an additional monodentate ligand, such as PyO. For **2a**, the iron center is bound to the tridentate ligand $\mathrm{Tp}^{t-\mathrm{Bu},i-\mathrm{Pr}}$ and assumed to be four-coordinate due to steric crowding around the metal site. This is supported by DFT calculations.[37] The coordination numbers of **2b**,**c** are uncertain, depending on whether the available sixth site is occupied by the PrCN solvent. Broad preedge peaks and low coordination numbers for the principal shell of N-donors from EXAFS fits **(**discussed in a later section) suggest that the solutions of **2b**,**c** likely consist of a mixture of unsolvated five-coordinate and solvated six-coordinate species. On the other hand, the iron center in **2c′** is very likely to be six-coordinate due to the introduction of PyO, whose coordination to the iron center is indicated by the blue-shift of the visible LMCT absorption band.

X-ray Absorption Near-Edge Structures. The X-ray absorption spectra of $[\mathrm{Fe^{III}(Tp^{\mathit{t}-Bu,\mathit{i}-Pr})(OO^{\mathit{t}}Bu)}]^{+}$, **2a**, $[\mathrm{Fe^{III}(6\text{-}Me_2\text{-}BPMCN)(OO^{\mathit{t}}Bu)(solv)}]^{2+}$, **2b**, $[\mathrm{Fe^{III}(L^8Py_2)(OO^{\mathit{t}}Bu)(solv)}]^{2+}$, **2c**, and $[\mathrm{Fe^{III}(L^8Py_2)(OO^{\mathit{t}}Bu)(OPy)}]^{2+}$, **2c′**, in the near-edge region are shown in Figure 3A. The position of the rising K-edge, assigned as the edge energy E_0, has been determined by the first inflection point of the first derivative of the spectra, representing the transition of a 1s electron to the continuum. The edge energy is mainly dependent on the effective charge of the iron, namely the oxidation state, and the coordination environment of the metal center. [The occurrence of additional transitions, such as 1s → 4p transitions, can further complicate the comparison of edge energies and give rise to multiple inflection points.[23]]

The edge energies of complexes **2a**−**c′** span a range of 3.7 eV, from 7122.0 to 7125.7 eV. Since complexes **2a**−**c′** have the same oxidation state, the variation in the edge energies must arise from the different coordination environments around the iron centers. Table 1 compares the edge and preedge information for the high-spin $\mathrm{Fe^{III}OOR}$ complexes reported here as well as those of previously described low-spin $\mathrm{Fe^{III}OOR(H)}$ complexes.[14] The edge energy for **2a**, 7122.0 eV, is the lowest among these complexes, perhaps due to its low coordination number and the consequent increased covalency of the Fe−OOR bond. Meanwhile those of **2b**,**c** fall near the average of the complexes listed in Table 1; the edge energy for **2c′** is 7125.7 eV, the highest value thus far reported for $\mathrm{Fe^{III}OOR(H)}$ complexes. The 2.1 eV upshift relative to the value for **2c** very likely is a result of the binding of the PyO ligand trans to the *tert*-butylperoxo group.

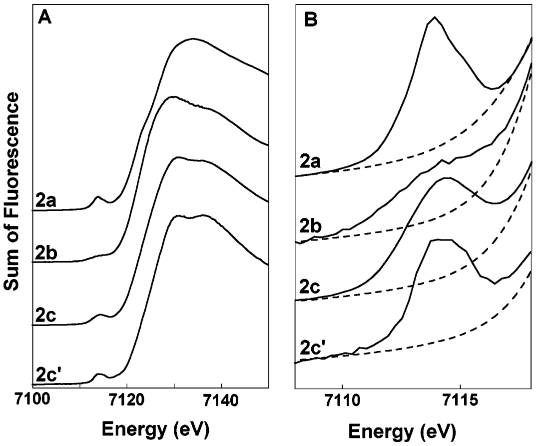

Figure 3. Fe K-edge X-ray absorption near-edge structures (XANES, fluorescence excitation) of $[\mathrm{Fe^{III}(Tp^{\mathit{t}-Bu,\mathit{i}-Pr})(OO^{\mathit{t}}Bu)}]^{+}$ (**2a**), $[\mathrm{Fe^{III}(6\text{-}Me_2\text{-}BPMCN)(OO^{\mathit{t}}Bu)(solv)}]^{2+}$ (**2b**), $[\mathrm{Fe^{III}(L^8Py_2)(OO^{\mathit{t}}Bu)(solv)}]^{2+}$ (**2c**), and $[\mathrm{Fe^{III}(L^8Py_2)(OO^{\mathit{t}}Bu)(OPy)}]^{2+}$ (**2c′**) [experimental data (—); background function (---)].

The preedge regions of **2a**−**c′** are magnified in Figure 3B and show peaks arising from the 1s → 3d transition. Those for **2a**,**c**,**c′** are relatively sharp, while that for **2b** is broader and not as prominent. These preedge peaks can be fit by Gaussian curves, and Table 1 summarizes the position (E_{preedge}), intensity (area), and line width at half-height of each complex. Despite a 3.7 eV spread of edge energies, the positions of preedge peaks of all four complexes are quite uniform and located near 7114 eV, reflecting the comparable effects of the coordination environment on the 1s and 3d orbitals. The preedge areas average about 21 units, and no clear trend can be discerned within this subset of four complexes that can be based only on coordination number. In fact the preedge area for 4-coordinate **2a** is the same as that for 6-coordinate **2c′**. Note also that these values are significantly higher than those found for low-spin iron(III)−η^1-peroxo and high-spin iron(III)−η^2-peroxo complexes (average 14−15 units; see Table 1).[14,40−42] It would thus appear that the previously well-established correlation between preedge area and coordination number derived from a database of simple coordination complexes[43,44] breaks down when applied to these high-spin iron(III)−peroxo complexes.

---

(38) Bukowski, M. R.; Halfen, H. L.; van den Berg, T. A.; Halfen, J. A.; Que, L., Jr. *Angew. Chem., Int. Ed.* **2005**, *44*, 584−587.

(39) Abbreviations used: BPMCN = *N*,*N′*-bis(pyridin-2-ylmethyl)-*N*,*N′*-dimethyl-*trans*-1,2-diaminocyclohexane; BPPE = *N*,*N*-bis((2-methylpyridin-6-yl)methyl)-3-aminopropionate; $\mathrm{H_2BPPA}$ = *N*-(pyridin-2-ylmethyl)bis((6-pivalamidopyridin-2-yl)methyl)amine; Me-TPEN = *N*-methyl-*N*,*N′*,*N′*-tris(pyridin-2-ylmethyl)ethane-1,2-diamine; N2Py2 = dimethyl(3,7-dimethyl-9,9-dihydroxy-2,4-bis(2-pyridyl)-3,7-diazabicyclononan-1,5-dicaboxylate); N2Py3 = dimethyl(7-methyl-9,9-dihydroxy-2,4-bis(2-pyridyl)-3-(2-pyridylmethyl)-3,7-diazabicyclononane-1,5-dicaboxylate); N4Py = *N*,*N*-bis(2-pyridylmethyl)-*N*-bis(2-pyridyl)methylamine; N-Et-HPTB = *N*,*N*,*N′*,*N′*-tetrakis[2′-(1′-ethylbenzimidazolyl)]-1,3-diamino-2-hydroxypropane; Ph-BIMP = 2,6-bis[bis{{2-(1-methyl-4,5-diphenylimidazolyl)methyl}amino}methyl]-4-methylphenolate; Hqn = quinaldic acid; $\mathrm{S^{Me2}N_4(tren)}$ = *N*,*N*-bis-(2-aminoethyl)-*N′*-(1,2-dimethyl-2-mercaptopropylene)ethane-1,2-diamine; $\mathrm{Tp}^{i-\mathrm{Pr},i-\mathrm{Pr}}$ = hydrotris(3,5-diisopropyl-1-pyrazolyl)borate; TPA = tris(2-pyridylmethyl)amine; 6-$\mathrm{Me_3}$-TPA = tris((2-methylpyridin-6-yl)methyl)amine.

(40) Bukowski, M. R.; Zhu, S.; Koehntop, K. D.; Brennessel, W. W.; Que, L., Jr. *J. Biol. Inorg. Chem.* **2004**, *9*, 39−48.

(41) Koehntop, K. D.; Rohde, J.-U.; Costas, M.; Que, L., Jr. *Dalton Trans.* **2004**, 3191−3198.

(42) Shearer, J.; Scarrow, R. C.; Kovacs, J. A. *J. Am. Chem. Soc.* **2002**, *124*, 11709−11717.

Table 1. XAS Preedge Peak Energies and Intensities for FeOOR(H) Complexes[a]

complex	E_0 (eV)	CN	E_{preedge} (eV)	area	width (eV)	ref
Low-Spin Fe^{III}(OOR(H)) Complexes[b]						
$[Fe^{III}(TPA)(OO^tBu)(solv)]^{2+}$	7123.6	6	7113.4	7.2	2.1	14
			7115.9	1.7	2.9	
$[Fe^{III}(N4Py)(OO^tBu)]^{2+}$	7123.4	6	7113.5	9.7	2.4	14
			7116.0	5.3	2.3	
$[Fe^{III}(N4Py)(OOH)]^{2+}$	7123.1	6	7113.5	9.9	2.4	41
			7116.1	5.3	2.4	
$[Fe^{III}(Me\text{-}TPEN)(OOH)]^{2+}$	7123.6	6	7113.6	9.0	2.3	41
			7116.0	5.1	2.2	
$[Fe^{III}(S^{Me2}N_4(tren))(OOH)]^{+}$	7123.7	6	7113.7	19	-	42
$[Fe^{III}(PaPy_3)(OOH)]^{+}$	7123.2	6	7114.0	11.8	3.9	40
High-Spin Fe^{III}(OOR(H)) Complexes						
$[Fe^{III}(Tp^{t-Bu,i-Pr})(OO^tBu)]^{+}$ (**2a**)	7122.0	4	7113.9	22	2.7	c
$[Fe^{III}(6\text{-}Me_2\text{-}BPMCN)(OO^tBu)(solv)]^{2+}$ (**2b**)	7122.8	5/6	7114.2	16	4.7	c
$[Fe^{III}(L^8Py_2)(OO^tBu)(solv)]^{2+}$ (**2c**)	7123.6	5/6	7114.2	23	3.7	c
$[Fe^{III}(L^8Py_2)(OO^tBu)(OPy)]^{2+}$ (**2c′**)	7125.7	6	7114.4	22	3.3	c
$[Fe^{III}(N4Py)(\eta^2\text{-}O_2)]^{+}$	7123.3	7	7114.0	16.0	4.6	41
$[Fe^{III}(Me\text{-}TPEN)(\eta^2\text{-}O_2)]^{+}$	7123.8	6/7	7114.3	13.7	3.9	41
			7117.4	1.2	2.0	

[a] For abbreviations, see ref 39. CN is coordination number. [b] The larger ligand field splittings of 3d orbitals of low-spin iron(III) complexes can give rise to more than one preedge feature.[46] [c] This work.

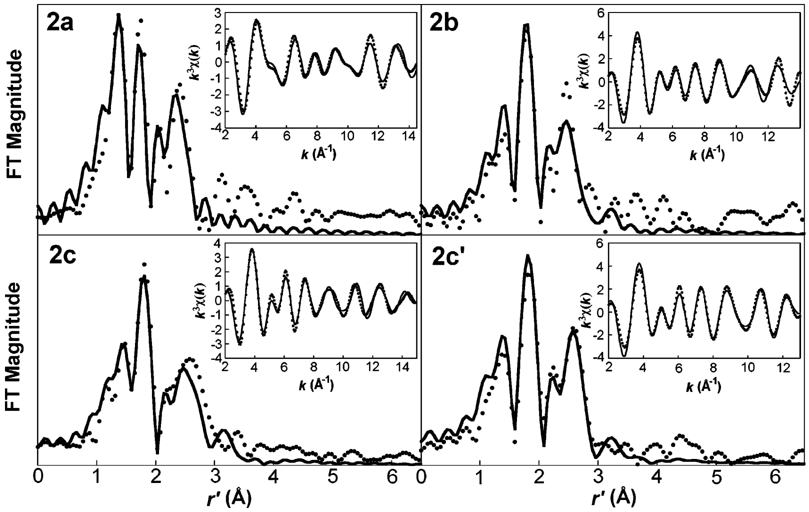

Figure 4. Fourier transforms of the Fe K-edge EXAFS data ($k^3\chi(k)$) and Fourier-filtered EXAFS spectra ($k^3\chi'(k)$, inset) for $[Fe^{III}(Tp^{t-Bu,\ i-Pr})(OO^tBu)]^+$ (**2a**, Fourier transform range, $k = 2{-}14.9$ Å^{-1}; back-transform range, $r' = 0.60{-}3.85$ Å; fit with parameters listed in fit no. **2a**-6 in Table 2), $[Fe^{III}(6\text{-}Me_2\text{-}BPMCN)(OO^tBu)(solv)]^{2+}$ (**2b**, Fourier transform range, $k = 2{-}14$ Å^{-1}; back-transform range, $r' = 0.60{-}3.50$ Å; fit with parameters listed in fit no. **2b**-8 in Table 2), $[Fe^{III}(L^8Py_2)(OO^tBu)(solv)]^{2+}$ (**2c**, Fourier transform range, $k = 2{-}14.9$ Å^{-1}; back-transform range, $r' = 0.70{-}3.80$ Å; fit with parameters listed in fit no. **2c**-8 in Table 2), and $[Fe^{III}(L^8Py_2)(OO^tBu)(OPy)]^{2+}$ (**2c′**, Fourier transform range, $k = 2{-}13$ Å^{-1}; back-transform range, $r' = 0.70{-}3.75$ Å; fit with parameters listed in fit no. **2c′**-8 in Table 2).

This discrepancy suggests that additional factors such as metal−ligand covalency could increase the mixing of 3d and 4p orbitals and further enhance preedge intensities.[45]

EXAFS Spectra and Fitting Results. Four prominent features at $r' > 1.2$ Å of varying magnitudes can be observed in the Fourier-transformed (r' space) Fe K-edge EXAFS data of the four high-spin (alkylperoxo)iron(III) complexes, **2a**−**c′** (Figure 4). These features can be best fit with two N/O shells in the first coordination sphere and one or two C shells in the second coordination sphere. The shorter Fe−N/O shell can be assigned to the Fe−O bond distance of the Fe−OOR unit, while the longer Fe−N/O shell can be associated mainly with the N scatterers of the polydentate supporting ligands.

The fitting results for all four complexes were obtained by following the standard procedures described in the Experimental Section and summarized in Table 2. The r' space spectrum of **2a** exhibits features at 1.4, 1.8, 2.1, and 2.4 Å (Figure 4 (**2a**)). These features are best fit with a combination of 1 N/O scatterer at 1.86 Å, 2 N/O scatterers at 2.05 Å, and 4 C scatterers at 2.90 Å (Table 2, fit no. **2a**-6), which correspond respectively to the O atom of the alkylperoxo ligand, the nitrogen atoms of the Tp ligand, and the C and N atoms α to the ligating N atoms of the Tp ligand. The smaller coordination number for the 2.05-Å shell probably reflects the distribution of Fe−N distances that gives rise to a Debye−Waller factor ($\Delta\sigma^2$) value larger than

---

(43) Westre, T. E.; Kennepohl, P.; DeWitt, J. G.; Hedman, B.; Hodgson, K. O.; Solomon, E. I. *J. Am. Chem. Soc.* **1997**, *119*, 6297−6314.

(44) Roe, A. L.; Schneider, D. J.; Mayer, R. J.; Pyrz, J. W.; Widom, J.; Que, L., Jr. *J. Am. Chem. Soc.* **1984**, *106*, 1676−1681.

(45) DeBeer George, S.; Brant, P.; Solomon, E. I. *J. Am. Chem. Soc.* **2005**, *127*, 667−674.

(46) Westre, T. E.; Kennepohl, P.; DeWitt, J. G.; Hedman, B.; Hodgson, K. O.; Solomon, E. I. *J. Am. Chem. Soc.* **1997**, *119*, 6297−6314.

Table 2. EXAFS Fitting Results for $[Fe^{III}(Tp^{t-Bu,i-Pr})(OO^tBu)]^+$, **2a**, $[Fe^{III}(6\text{-}Me_2-BPMCN)(OO^tBu)(solv)]^{2+}$, **2b**, $[Fe^{III}(L^8Py_2)(OO^tBu)(solv)]^{2+}$, **2c**, and $[Fe^{III}(L^8Py_2)(OO^tBu)(OPy)]^{2+}$, **2c′** [a]

		Fe−N/O			Fe−N/O			Fe···C			Fe···C			
complex	fit	*n*	*r*/Å	$\Delta\sigma^2$	*n*	*r*/Å	$\Delta\sigma^2$	*n*	*r*/Å	$\Delta\sigma^2$	*n*	*r*/Å	$\Delta\sigma^2$	GOF $10^3\epsilon^2$
2a	1				5	1.97	29							0.72
	2				4	1.97	23							0.73
	3	1	1.84	0.7	4	2.04	15							0.64
	4	1	1.84	0.3	3	2.05	9.3							0.59
	5	1	1.86	0.3	2	2.06	4.6							0.57
	6	**1**	**1.86**	**0.2**	**2**	**2.05**	**4.7**	**4**	**2.90**	**6.3**				**0.41**
	7	1	1.84	0.3	3	2.04	9.4	4	2.90	6.5				0.49
2b	1				6	2.16	27							1.09
	2				5	2.16	21							1.09
	3	1	1.92	−0.8	5	2.19	10.7							0.85
	4	2	1.94	4.9	4	2.20	5.1							0.91
	5	1	1.93	−0.5	4	2.19	7.4							0.83
	6	2	1.96	7.0	3	2.20	2.6							0.91
	7	1	1.93	−0.7	4	2.18	7.8	7	2.98	8.6				0.59
	8	**1**	**1.93**	**−0.6**	**4**	**2.18**	**7.6**	**7**	**2.99**	**9.0**	**4**	**3.54**	**10**	**0.51**
2c	1				6	2.13	26							0.85
	2				5	2.14	21							0.85
	3	1	1.93	1.3	5	2.17	10.9							0.75
	4	2	1.95	7.5	4	2.19	6.9							0.73
	5	1	1.94	1.5	4	2.18	7.6							0.71
	6	1	1.96	2.2	3	2.18	4.5							0.70
	7	1	1.95	2.0	3	2.18	4.7	5	3.02	8.0				0.49
	8	**1**	**1.95**	**2.1**	**3**	**2.18**	**4.6**	**5**	**3.02**	**8.0**	**4**	**3.57**	**8.0**	**0.36**
	9	1	1.94	1.4	4	2.17	7.6	5	3.03	8.1	4	3.57	8.0	0.42
2c′	1				6	2.14	29							1.26
	2				5	2.15	25							1.27
	3	1	1.94	−1.5	5	2.20	10							1.00
	4	2	1.96	3.4	4	2.22	4.3							0.93
	5	1	1.95	−1.2	4	2.21	6.6							0.97
	6	2	1.98	5.0	3	2.22	1.6							0.91
	7	2	1.96	3.4	4	2.21	4.6	6	3.06	4.5				0.57
	8	**2**	**1.96**	**3.4**	**4**	**2.21**	**4.5**	**6**	**3.06**	**4.6**	**4**	**3.59**	**9.0**	**0.44**
	9	1	1.95	−1.2	4	2.20	6.9	6	3.06	4.4	4	3.59	9.0	0.51

[a] Fourier transformed range for **2a** and **2c**: $k = 2-14.9$ Å^{-1} (resolution 0.12 Å); for **2b**: $k = 2-14$ Å^{-1} (resolution 0.13 Å); for **2c′**: $k = 2-13$ Å^{-1} (resolution 0.14 Å). *r* is in units Å, $\Delta\sigma^2$ in 10^{-3} Å^2. Back-transformation range for **2a**: $r' = 0.60-3.85$ Å; for **2b**: $r' = 0.60-3.50$ Å; for **2c**: $r' = 0.70-3.80$ Å; for **2c′**: $r' = 0.70-3.75$ Å.

typically accepted when a CN of 3 is used for the fit (Table 2, fit no. **2a**-7). Such a distribution of distances, ca. 0.17 Å, is in fact observed in crystal structures of $Fe(Tp^{t-Bu,i-Pr})$ complexes.[17]

The *r′* space spectrum of **2b** shows four similar features (Figure 4 (**2b**)) that can be fit by a combination of 1 N/O scatterer at 1.93 Å, 4 N/O scatterers at 2.18 Å, 7 C scatterers at 2.99 Å, and 4 C scatterers at 3.54 Å (Table 2, fit no. **2b**-8) with the 3.54-Å shell corresponding to the *β*-carbon atoms of the pyridine ligands. We note the longer iron−scatterer distances for **2b** than for **2a**, commensurate with an increase in the coordination number of the latter. It is however not clear whether the available sixth site is occupied by PrCN or not. It is likely that the sample solution consists of a mixture of 5- and 6-coordinate species as reflected by the broadness of the preedge peak relative to those of the other complexes and the larger Debye−Waller factor, $\Delta\sigma^2 = 7.6$, associated with the 2.18-Å shell that represents the N donors of the tetradentate ligand.

Like **2b**, the EXAFS spectrum of **2c** is also best fit with a combination of four shells: 1 N/O scatterer at 1.95 Å, 3 N/O scatterers at 2.18 Å, 5 C scatterers at 3.02 Å, and 4 C scatterers at 3.54 Å (Figure 3 (**2c**); Table 2, fit no. **2c**-8), a result consistent with its proposed structure. However, different results are obtained in fitting the EXAFS spectrum of **2c′** (Figure 3 (**2c′**); Table 2, fit no. **2c′**-8). Although four shells of scatterers are also required in the latter case at 1.96, 2.21, 3.06, and 3.59 Å, the short shell is consistently better fit with 2 N/O scatterers instead of 1. We assign the additional scatterer in the 1.96-Å shell to the oxygen atom of the added PyO ligand. This is quite a reasonable conclusion, given that the four crystallographically characterized iron(III) complexes of ligands closely related to pyridine *N*-oxide have Fe−O bond lengths of 1.98−2.04 Å.[47−49] When compared to the best fits of the other Fe−OOR complexes, the relatively large Debye−Waller factor, $\Delta\sigma^2 = 3.4$, associated with this shell can be rationalized with the presence of two similar but inequivalent Fe−O distances.

The EXAFS analyses of **2a**−**c′** reveal Fe−O bond lengths for these high-spin (alkylperoxo)iron(III) complexes that range from 1.86 to 1.96 Å. These distances are substantially longer than those found for low-spin (alkyl- and hydroperoxo)iron(III) complexes of related neutral polydentate ligands (1.76−1.78 Å, Table 3).[14,40−42,50] The longer Fe−O bonds

---

(47) Li, X.-L.; Niu, D.-Z.; Lu, Z.-S.; Shi, D.-Q.; Yu, K.-B. *Jiegou Huaxue* **2003**, *22*, 47−49.

(48) Van Albada, G. A.; Mutikainen, I.; Turpeinen, U.; Reedijk, J. *J. Chem. Crystallogr.* **2002**, *31*, 75−79.

(49) Scarrow, R. C.; Riley, P. E.; Abu-Dari, K.; White, D. L.; Raymond, K. N. *Inorg. Chem.* **1985**, *24*, 954−967.

(50) Roelfes, G.; Vrajmasu, V.; Chen, K.; Ho, R. Y. N.; Rohde, J.-U.; Zondervan, C.; la Crois, R. M.; Schudde, E. P.; Lutz, M.; Spek, A. L.; Hage, R.; Feringa, B. L.; Münck, E.; Que, L., Jr. *Inorg. Chem.* **2003**, *42*, 2639−2653.

Table 3. Structural Parameters of Fe(OOR(H)) Complexes[a]

complex	CN	$d_{\mathrm{Fe-O(peroxo)}}$[a]/Å	ν_{Fe}-O/cm^{-1} ($k_{\mathrm{Fe-O}}$/mdyn Å^{-1})	*ref*
Low-Spin $\mathrm{Fe^{III}(OOR(H))}$ Complexes				
$[\mathrm{Fe^{III}(N4Py)(OOH)}]^{2+}$	6	1.76	632 (3.62)	50, 51
$[\mathrm{Fe^{III}(TPA)(OO^{\mathit{t}}Bu)(solv)}]^{2+}$	6	1.78	696 (3.53)	14, 52
$[\mathrm{Fe^{III}(N4Py)(OO^{\mathit{t}}Bu)}]^{2+}$	6	1.78		14
$[\mathrm{Fe^{III}(N2Py2)(OO^{\mathit{t}}Bu)(NCMe)}]^{2+}$	6	*1.78*	694	53
$[\mathrm{Fe^{III}(BPMCN)(OO^{\mathit{t}}Bu)(solv)}]^{2+}$	6	1.81	685	11
$[\mathrm{Fe^{III}(Me\text{-}TPEN)(\eta^{1}\text{-}OOH)}]^{2+}$	6	1.81		41
$[\mathrm{Fe^{III}(S^{Me2}N_4(tren))(OOH)}]^{+}$	6	1.86		42
High-Spin $\mathrm{Fe^{III}(OOR(H))}$ Complexes				
$[\mathrm{Fe^{III}(Tp^{\mathit{t}-Bu,\mathit{i}-Pr})(OO^{\mathit{t}}Bu)}]^{+}$ (**2a**)	4	1.86	625 (2.19)	35, 37, *b*
E47A SOR + $\mathrm{H_2O_2}$ ($\mathrm{Fe^{III}-OO(H)}$)	6	*1.87*	438	54, 55
E114A SOR + $\mathrm{H_2O_2}$($\mathrm{Fe^{III}-OOH}$)	6	2.0	567	8b
$[\mathrm{Fe^{III}(N2Py2)(OO^{\mathit{t}}Bu)}]^{2+}$	5/6	1.91	650	53
$[\mathrm{Fe^{III}(6\text{-}Me_2BPMCN)(OO^{\mathit{t}}Bu)}]^{2+}$ (**2b**)	5/6	1.93	635	b
$[\mathrm{Fe^{III}(qn)_2(OOC(O)O)}]^{-}$	6	1.936	547,578	56
$[\mathrm{Fe^{III}(6\text{-}Me_3\text{-}TPA)(OO^{\mathit{t}}Bu)(solv)}]^{2+}$	5/6	*1.94*	637 (2.87)	15, 34
$[\mathrm{Fe^{III}(L^{8}Py_2)(OO^{\mathit{t}}Bu)(solv)}]^{2+}$ (**2c**)	5/6	1.95	627	38, *b*
$[\mathrm{Fe^{III}(L^{8}Py_2)(OO^{\mathit{t}}Bu)(OPy)}]^{+}$ (**2c′**)	6	1.96	623	38, *b*
purple lipoxygenase (1IK3)	6	2.01		9
oxyhemerythrin (Fe−O−Fe−OOH)(1HMO)	6	2.09	503	57, 58
$[\mathrm{Fe^{III}(H_2BPPA)(OOH)}]^{2+}$	6		621	59
High-Spin $\mathrm{Fe^{III}(\eta^{2}\text{-}OO)}$ Complexes				
$[\mathrm{Fe^{III}(N4Py)(OO)}]^{+}$	7	1.93	495	50
$[\mathrm{Fe^{III}(Me\text{-}TPEN)(OO)}]^{+}$	6/7	1.99	470	41
$[\mathrm{Fe^{III}(N2Py3)(OO)}]^{+}$	6	*1.91*	493	60
NDO/indole/$\mathrm{O_2}$ complex (1NDO)	6	1.7, 2.0		10
High-Spin (μ-1,2-Peroxo)diiron(III) Complexes				
$[\mathrm{Fe^{III}{}_2(O_2)(N\text{-}Et\text{-}HPTB)(Ph_3PO)_2}]^{3+}$	6	1.881		61
$[\mathrm{Fe^{III}{}_2(O_2)(O_2CPh)(Ph\text{-}BIMP)}]^{2+}$	6	1.863, 1.943		62
$[\mathrm{Fe^{III}{}_2(O_2)(O_2CCH_2Ph)_2(Tp^{\mathit{i}-Pr,\mathit{i}-Pr})_2}]$	6	1.878	421 (1.99)	63, 64
$[\mathrm{Fe^{III}{}_2(O_2)(OH)(BPPE)_2}]^{+}$	6	1.877	460 (2.18)	65
$[\mathrm{Fe^{III}{}_2(O_2)(O)(6\text{-}Me_3\text{-}TPA)_2}]^{3+}$	6	1.84	462	66

[a] For abbreviations, see ref 39. Distances for synthetic complexes with two decimal precision derive from EXAFS analysis, while those with three decimal precision derive from X-ray crystallography. Values in italics derive from DFT calculations. [b] This work.

for the high-spin complexes are to be expected because of the increase in the ionic radius of the iron(III) center upon changing from low spin to high spin. The larger range of Fe−O distances observed for the high-spin subset is also not surprising, since this spin state can accommodate a range of coordination numbers, 4 for **2a**, 5 or 6 for **2b**,**c**, and 6 for **2c′**. On the other hand, the low-spin configuration requires a coordination number of 6. Not surprisingly, the short 1.86-Å bond length is associated with 4-coordinate **2a**, while the long 1.96-Å bond length corresponds to 6-coordinate **2c′**.

Resonance Raman spectroscopy has been shown to be useful for distinguishing between low-spin and high-spin (alkylperoxo)iron(III) complexes.[2,34] The Raman signature for a low-spin complex consists of a $\nu_{\mathrm{Fe-O}}$ near 700 cm^{-1} and a $\nu_{\mathrm{O-O}}$ near 800 cm^{-1}, while the corresponding high-spin complex has $\nu_{\mathrm{Fe-O}}$ and $\nu_{\mathrm{O-O}}$ values near 600 and 900 cm^{-1}, respectively. These patterns have led us to suggest that a low-spin $\mathrm{Fe^{III}-OOR}$ complex has a stronger Fe−O bond and a weaker O−O bond than its high-spin counterpart. This notion has subsequently been substantiated by normal coordinate analyses of both low-spin and high-spin (alkylperoxo)iron(III) complexes.[15,52] However, when the Raman data for the four high-spin (alkylperoxo)iron(III) complexes in this study are compared in light of their respective Fe−O bond lengths (Table 3), we note a lack of a correlation between bond length and $\nu_{\mathrm{Fe-O}}$. The $\nu_{\mathrm{Fe-O}}$ frequencies for these four complexes differ by only 12 cm^{-1}, ranging from 623 to 637 cm^{-1}, despite the 0.1 Å difference in Fe−O distances observed for **2a**−**c′** (Table 3). In fact, the complex with the shortest Fe−O bond, **2a**, does not even have the highest value for $\nu_{\mathrm{Fe-O}}$. The normal coordinate analysis of the "$\nu_{\mathrm{Fe-O}}$" mode in $\mathrm{Fe^{III}-OO^{t}Bu}$ complexes shows that this mode consists mainly of an Fe−O stretching component that is coupled to one or more deformations of the *tert*-butoxy group,[37] which increases the frequency of this mode. In support, two out of three characterized high-spin $\mathrm{Fe^{III}-OOH}$ complexes have $\nu_{\mathrm{Fe-O}}$ modes near 500 cm^{-1},[54,57,59] as well as all of high-spin $\mathrm{Fe^{III}-OO-Fe^{III}}$ complexes.[67] Thus, some caution must be exercised in directly using Raman spectral

---

(51) Lehnert, N.; Neese, F.; Ho, R. Y. N.; Que, L., Jr.; Solomon, E. I. *J. Am. Chem. Soc.* **2002**, *124*, 10810−10822.

(52) Lehnert, N.; Ho, R. Y. N.; Que, L., Jr.; Solomon, E. I. *J. Am. Chem. Soc.* **2001**, *123*, 8271−8290.

(53) Bautz, J.; Comba, P.; Que, L., Jr. *Inorg. Chem.* **2006**, *45*, 7077−7082.

(54) Mathé, C.; Mattioli, T. A.; Horner, O.; Lombard, M.; Latour, J.-M.; Fontecave, M.; Nivière, V. *J. Am. Chem. Soc.* **2002**, *124*, 4966−4967.

(55) Silaghi-Dumitrescu, R.; Silaghi-Dumitrescu, I.; Coulter, E. D.; Kurtz, D. M., Jr. *Inorg. Chem.* **2003**, *42*, 446−456.

(56) Hashimoto, K.; Nagatomo, S.; Fujinami, S.; Furutachi, H.; Ogo, S.; Suzuki, M.; Uehara, A.; Maeda, Y.; Watanabe, Y.; Kitagawa, T. *Angew. Chem., Int. Ed.* **2002**, *41*, 1202−1205.

(57) Shiemke, A. K.; Loehr, T. M.; Sanders-Loehr, J. *J. Am. Chem. Soc.* **1984**, *106*, 4951−4956.

(58) Holmes, M. A.; Le Trong, I.; Turley, S.; Sieker, L. C.; Stenkamp, R. E. *J. Mol. Biol.* **1991**, *218*, 583−593.

(59) Wada, A.; Ogo, S.; Nagatomo, S.; Kitagawa, T.; Watanabe, Y.; Jitsukawa, K.; Masuda, H. *Inorg. Chem.* **2002**, *41*, 616−618.

(60) Bukowski, M. R.; Comba, P.; Limberg, C.; Merz, M.; Que, L., Jr.; Wistuba, T. *Angew. Chem., Int. Ed.* **2004**, *43*, 1283−1287.

(61) Dong, Y.; Yan, S.; Young, V. G., Jr.; Que, L., Jr. *Angew. Chem., Int. Ed.* **1996**, *35*, 618−620.

data for iron(III)−peroxo complexes to infer Fe−O bond strength. Force constants derived from the normal coordinate analysis more closely reflect these bond strengths.[34,37,51,52,64,65]

The XAS studies of the four synthetic high-spin (alkylperoxo)iron(III) complexes reported here, **2a**−**c′**, show that they have longer Fe−O bonds than their low-spin counterparts. The latter complexes with supporting tetradentate TPA and BPMCN ligands undergo O−O bond homolysis and convert quantitatively to high-valent oxoiron(IV) species in first-order decay processes.[11,13] In contrast, high-spin complexes with related tetradentate ligands exhibit a more complicated thermal decay and no high-valent species has yet been identified among the decay products. As pointed out earlier,[15] the stronger Fe−O and weaker O−O bonds of the low-spin complexes very likely decrease the energy barrier for O−O bond cleavage and promote their conversion to oxoiron(IV) species. By the same argument, O−O bond cleavage will not be as favored for corresponding high-spin (alkylperoxo)iron(III) complexes since they have weaker Fe−O and stronger O−O bonds. Nevertheless such transformations must take place for the high-spin peroxoiron(III) species observed in the oxygen activation cycles of the Rieske dioxygenases, methane monooxygenase, and ribonucleotide reductase,[2−4] so some additional mechanistic feature(s) must be needed to overcome the activation barrier for O−O bond cleavage in these active sites. Efforts under way are aimed to identify the factors that promote O−O cleavage in high-spin peroxoiron(III) complexes.

Acknowledgment. This work was supported by grants from the National Institutes of Health Grant (GM-38767 to L.Q.), the Japan Society for the Promotion of Science (17350043 to K.F.), and a fellowship from the Deutsche Forschungsgemeinschaft (to J.-U.R.). XAS data were collected on beamline 9-3 at the Stanford Synchrotron Radiation Laboratory (SSRL) and beamline X9B at the National Synchrotron Light Source (NSLS). The SSRL Structural Molecular Biology Program is supported by the Department of Energy, Office of Biological and Environmental Research, and by the National Institutes of Health, National Center for Research Resources, Biomedical Technology Program. NSLS is supported by the U.S. Department of Energy, Office of Science, Office of Basic Energy Sciences, under Contract No. DE-AC02-98CH10886.

IC700649W

---

(62) Ookubo, T.; Sugimoto, H.; Nagayama, T.; Masuda, H.; Sato, T.; Tanaka, K.; Maeda, Y.; Okawa, H.; Hayashi, Y.; et al. *J. Am. Chem. Soc.* **1996**, *118*, 701−702.

(63) Kim, K.; Lippard, S. J. *J. Am. Chem. Soc.* **1996**, *118*, 4914−4915.

(64) Brunold, T. C.; Tamura, N.; Kitajima, N.; Moro-Oka, Y.; Solomon, E. I. *J. Am. Chem. Soc.* **1998**, *120*, 5674−5690.

(65) Zhang, X.; Furutachi, H.; Fujinami, S.; Nagatomo, S.; Maeda, Y.; Watanabe, Y.; Kitagawa, T.; Suzuki, M. *J. Am. Chem. Soc.* **2005**, *127*, 826−827.

(66) Dong, Y.; Zang, Y.; Kauffmann, K.; Shu, L.; Wilkinson, E. C.; Münck, E.; Que, L., Jr. *J. Am. Chem. Soc.* **1997**, *119*, 12683−12684.

(67) Girerd, J.-J.; Banse, F.; Simaan, A. J. *Struct. Bond.* **2000**, *97*, 145−177.